

AN EXPLORATION OF ADVANCED SLW MODELING APPROACHES IN COMPREHENSIVE COMBUSTION PREDICTIONS

J. Badger, B.W. Webb*, and V.P. Solovjov

webb@byu.edu

Department of Mechanical Engineering, Brigham Young University
Provo, UT 84602 USA

Abstract

Recently, work was published demonstrating the integration of the Spectral Line Weighted-sum-of-gray-gases model for advanced modeling of gas radiation in high temperature gases in a comprehensive combustion modeling prediction scheme. This prior work compared predictions using the Reference Approach SLW model with the Domain Based Weighted-Sum-of-Gray-Gases model used in Fluent. This work reports on the implementation of the Rank Correlated SLW model and the Locally Correlated SLW model in the combustion scenario studied in an earlier work, complementing the Reference Approach SLW model predictions reported previously. The predictions confirm the need for such advanced radiation modeling to accurately resolve the radiative flux divergence and temperature fields, particularly in localized regions of the flame zone where very large differences in temperature and radiative heating may be found relative to the more rudimentary modeling approach. Results also demonstrate the dependence of the predictions for all three SLW model variants on the number of gray gases employed in the simulations. The predictions reveal that the Rank Correlated SLW model is perhaps the most robust of all models.

Introduction

The Advanced Spectral Line Weighted-Sum-of-Gray-Gases (SLW) model is a so-called global method for simulation of radiation transfer, and is based on the work of Denison and Webb [1]. The SLW model was first developed and published in 1993 for single-component, isothermal gas systems, and has been refined to treat multicomponent, non-homogeneous, non-isothermal systems. The model has been demonstrated to produce solutions accurate to within a few percent of rigorous line-by-line benchmark predictions at a computational cost that is a tiny fraction (typically 0.001%) of the cost of line-by-line predictions. A recent publication explored the implementation of the advanced SLW model for predicting radiative transfer from high temperature gases in a Fluent-based comprehensive turbulent-flow combustion prediction methodology [2].

There has been only limited prior work in the literature reporting the use of the SLW gas radiation model in comprehensive combustion predictions. That work was detailed previously [2], and will not be repeated here. Suffice it to say that the work of Nguen *et al.* [3], Garten [4], Rebola and Azevedo [5], and Krishnamoorthy *et al.* [6] have explored the use the SLW model in comprehensive combustion predictions. The more recent work of Darbandi *et al.* [7] has added to the body of related work.

SLW Modelling of Radiative Transfer in Gases

Propagation of thermal radiation in gaseous media with spectral absorption coefficient $\kappa_\eta(\phi) = N(\phi)C_\eta(\phi)$ is characterized by the intensity of radiation $I_\eta(s, \Omega)$ at wavenumber η along a path s in a direction Ω . Here, $C_\eta(\phi)$ is the local absorption cross-section, and

$N(\phi)$ is the molar density at the local gas thermodynamic state, symbolically denoted by the composite vector $\phi = \{T, p, Y_i\}$ which includes the temperature T , total pressure p , and species mole fractions Y_i . The detailed continuous gas absorption cross-section $C_\eta(\phi)$ can include millions of spectral lines with complex dependence on the local thermodynamic state. The SLW spectral model replaces the absorption cross-section by a piece-wise constant histogram spectrum $C_\eta(\phi) = C_j$, $\eta \in \Delta_j$, where $\Delta_j = \{\eta : \tilde{C}_{j-1} < C_\eta(\phi) < \tilde{C}_j\}$ are the gray gas spectral intervals defined by supplemental cross-sections \tilde{C}_j , $j = 0, 1, 2, \dots, n$, n is the number of gray gases in the model, C_j are the gray gas absorption cross-sections, and a_j are the corresponding weights describing the contribution of each gray gas to the total radiative transfer. The weights a_j are calculated using the Absorption Line Blackbody Distribution Function (ALBDF) [8,9]. Integrating the spectral RTE over spectral intervals Δ_j (provided that these intervals are maintained the same for all spatial locations s) yields the gray gas RTEs [10]

$$\partial I_j(s, \Omega)/\partial s = -\kappa_j(s)I_j(s, \Omega) + a_j(s)\kappa_j(s)I_b[T(s)] \quad (1)$$

The ALBDF $F(C, \phi, T_b)$ as a function of continuous variable C is defined as the fraction of the total blackbody emissive power $E_b(T_b) = \sigma T_b^4$ emitted at source temperature T_b that lies in the part of the spectrum where $C_\eta(\phi)$ is below a prescribed value C [1,9]. The ALBDF is a strictly increasing function of the variable C and is therefore invertible, with the inverse ALBDF expressed as a function of the continuous F -variable as $C = C(F, \phi, T_b)$. The ALBDF has been calculated from the detailed absorption cross-section for a range of temperatures, partial pressures (where appropriate), and total pressures for H₂O, CO₂, and CO using the HITEMP 2010 spectroscopic database, and has been tabulated [11].

In non-isothermal/non-homogeneous gas media the thermodynamic state $\phi(s)$ varies with location s . To avoid appearance of additional so-called Leibnitz terms of integration of the RTE over the spectrum, the spectral intervals of integration $\Delta_j = \{\eta : \tilde{C}_{j-1} < C_\eta(\phi(s)) < \tilde{C}_j\}$ must be maintained the same for all spatial locations s . These additional Leibnitz terms can be ignored, incurring error, or they can be eliminated by maintaining the spectral intervals Δ_j constant at all locations by invoking the correlated SLW model assumptions [9,10].

The assumption of a rank correlated spectrum applied to the SLW model is formulated as follows [12,13]. For any set of gray gas supplemental absorption cross-sections \tilde{C}_j^1 prescribed at a location for gas thermodynamic state ϕ_1 , there exists a set of cross-sections \tilde{C}_j^2 such that

$$\{\eta : C_\eta(\phi_1) < \tilde{C}_j^1\} = \{\eta : C_\eta(\phi_2) < \tilde{C}_j^2\} = \tilde{\Delta}_j \quad (2)$$

The spectral intervals defined by the cross-sections \tilde{C}_j^2 at state 2 and those defined by \tilde{C}_j^1 at state 1 are the same. These wavenumber intervals are denoted $\tilde{\Delta}_j$. Therefore, the equality

$$F(\tilde{C}_j^1, \phi_1, T_b) = F(\tilde{C}_j^2, \phi_2, T_b) \text{ for } j = 1, 2, 3, \dots, n \quad (3)$$

relating the ALBDF of the rank correlated gray gas supplemental absorption cross-sections \tilde{C}_j^1 and \tilde{C}_j^2 at any two arbitrary thermodynamic states ϕ_1 and ϕ_2 is always satisfied when the same blackbody source temperature T_b is prescribed for both sides of Eq. (3). This provides the same fraction of the total blackbody emissive power $E_b(T_b)$ at source temperature T_b in the same spectral intervals $\tilde{\Delta}_j$ at the two thermodynamic states. The implicit equation (3) relates the supplemental absorption cross-sections which preserve the gray gas wavenumber intervals at different thermodynamic states. Different SLW approaches vary by the choice of the gray gas supplemental cross-sections \tilde{C}_j and the blackbody source temperature T_b used in Eq. (3), and were introduced in [12]. They are distinguished by the manner in which the blackbody source temperature T_b in Eq. (3) is specified, and by the different approaches for determining the local gray gas absorption cross-sections. SLW methods for which T_b is fixed for all locations in the medium are the original RA-SLW model and the RC-SLW model pre-

sented and explored in detail elsewhere [9,12]. Those for which the blackbody source temperature is the local gas temperature $T_b = T_{loc}$ are termed “locally correlated” models. Recently the Locally Correlated SLW model (LC-SLW) was presented and investigated in detail in [14], and compared to other SLW model variants. It should be noted that Eqs. (2) and (3), which are used for construction of the correlated SLW models, are exactly valid for rigorously correlated/comonotonic gas spectra. In this case, the conservation of the spectral intervals for different thermodynamic states is rigorously preserved and the relations are exact. However, real gas spectra are not perfectly correlated, and therefore, the local cross-sections constructed using Eq. (3) may not generate the same spectral intervals Δ_j at different gas thermodynamic states. Thus, all reference approaches are approximations for real gas spectra. Because of this, the different correlated SLW versions can perform differently.

Outline of Correlated SLW Approaches

Construction of the local spectral model in the SLW method consists in finding the local values of the gray gas absorption coefficients and their weights in the gray gas RTE, Eq. (1):

$$\kappa_j^{loc} = \kappa_j(s), \quad a_j^{loc} = a_j(s) \quad (4)$$

The following notation in outline of the SLW approaches is used for the local parameters

$$\phi_{loc} = \phi(s) = \{T_{loc} = T(s), p_{loc} = p(s), Y_{i,loc} = Y_{i,loc}(s)\} \quad (5)$$

and for the arbitrary chosen reference parameters $\phi_{ref} = \{T_{ref}, p_{ref}, Y_{i,ref}\}$. Also, N^{loc} is the local gas molar density and Y^{loc} is the local gas specie mole fraction.

Division of the gray gases in the RA-SLW and LC-SLW methods consists of partitioning the C -variable into logarithmically evenly spaced supplemental absorption cross-sections, $\tilde{C}_j^{ref} = C_{min} (C_{max}/C_{min})^{j/n}$, $j = 0, 1, 2, \dots, n$ and absorption cross-sections $C_j^{ref} = (\tilde{C}_{j-1}^{ref} \tilde{C}_j^{ref})^{1/2}$, where C_{min} and C_{max} are chosen to effectively cover the entire absorption spectrum. Division of the gray gases for the RC-SLW method is performed by partitioning of the F -variable into supplemental values $0 \leq \tilde{F}_j^{ref} \leq 1$ and F_j^{ref} for $\tilde{F}_{j-1}^{ref} < F_j^{ref} < \tilde{F}_j^{ref}$, where Gauss-Legendre quadratures are used to define the subdivision.

The methodology for determining the local gray gas absorption coefficients (absorption cross-sections) and associated gray gas weights needed for the solution of the gray gas RTE Eq. (1) is outlined for each of the SLW models below.

Reference Approach SLW (RA-SLW) Model

The Reference Approach SLW model was first proposed in [9] as follows:

- 1) The reference values of the F -variable are calculated using the direct ALBDF:

$$\tilde{F}_j^{ref} = F(\tilde{C}_j^{ref}, \phi_{ref}, T_{ref}) \quad (6)$$

- 2) The local values of the supplemental absorption cross-sections and the local gray gas absorption coefficients are calculated using the inverse ALBDF:

$$\tilde{C}_j^{loc} = C(\tilde{F}_j^{ref}, \phi_{loc}, T_{ref}), \quad \kappa_j^{loc} = N^{loc} Y^{loc} \sqrt{\tilde{C}_{j-1}^{loc} \tilde{C}_j^{loc}} \quad (7)$$

- 3) The local gray gas weights are calculated using the ALBDF:

$$a_j^{loc} = F(\tilde{C}_j^{ref}, \phi_{ref}, T_{loc}) - F(\tilde{C}_{j-1}^{ref}, \phi_{ref}, T_{loc}) \quad (8)$$

Locally Correlated SLW (LC-SLW) Model

The Locally Correlated SLW model proceeds with the following steps [12,14]:

- 1) The local values of the F -variable and the local gray gas weights are calculated using the ALBDF:

$$\tilde{F}_j^{loc} = F(\tilde{C}_j^{ref}, \phi_{ref}, T_{loc}), \quad F_j^{loc} = F(C_j^{ref}, \phi_{ref}, T_{loc}), \quad a_j^{loc} = \tilde{F}_j^{loc} - \tilde{F}_{j-1}^{loc} \quad (9)$$

- 2) The local values of the absorption cross-sections and the local gray gas absorption coefficients are calculated using the inverse ALBDF:

$$C_j^{loc} = C(F_j^{loc}, \phi_{loc}, T_{loc}), \quad \kappa_j^{loc} = N^{loc} Y^{loc} C_j^{loc} \quad (10)$$

Rank Correlated SLW (RC-SLW) Model

In the Rank Correlated SLW model the reference blackbody source temperature T_b must first be chosen (the spatial average is used in this paper) [12,13]. Then the spectral model is constructed by the following two steps:

- 1) The local values of the supplemental absorption cross-sections and the local gray gas absorption coefficients are calculated using the inverse ALBDF:

$$\tilde{C}_j^{loc} = C(\tilde{F}_j^{ref}, \phi_{loc}, T_b), \quad C_j^{loc} = C(F_j^{ref}, \phi_{loc}, T_b), \quad \kappa_j^{loc} = N^{loc} Y^{loc} C_j^{loc} \quad (11)$$

- 2) and the local gray gas weights are calculated using the ALBDF:

$$a_j^{loc} = F(\tilde{C}_j^{loc}, \phi_{loc}, T_{loc}) - F(\tilde{C}_{j-1}^{loc}, \phi_{loc}, T_{loc}) \quad (12)$$

The principal difference between the methods may be summarized as follows. The RA-SLW method applies the reference condition for the gas state ϕ_{ref} and for the blackbody source temperature $T_b = T_{ref}$. The RC-SLW method avoids specification of the gas reference state ϕ_{ref} (while still specifying T_b), whereas the LC-SLW method avoids application of the reference value of the blackbody source temperature T_b (while still specifying T_{ref}). The greater the number of gray gases used in the prediction the higher the accuracy. Prior work has demonstrated theoretically that the RC-SLW model is the optimal correlated SLW model [12,13], and produces the greatest overall accuracy. However, additional study has revealed that the LC-SLW model may yield improved predictions in regions of high temperature [14].

Because the Weighted-Sum-of-Gray-Gases Model has been in use for a number of years, it bears brief description here. The classical WSGG model is formulated as the solution of multiple RTEs for fictitious “gray gases” and a fictitious “clear gas” to simulate the radiation heat transfer behavior of combustion gas mixtures. The total radiation intensity is then the summation of radiation intensity for all gray gases. In the classical WSGG Model the local gray gas absorption coefficients and their weights appearing in Eq. (1) are calculated through empirical fits of gas total emissivity data. Several sets of coefficients for the classical WSGG method are found in the literature. Because of the nature of the WSGG model formulation, WSGG coefficients are derived for specific H₂O - CO₂ partial pressures and pressure ratios corresponding to complete combustion of different fuels under one atmospheric pressure [2].

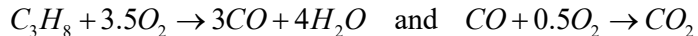
Problem Statement

The same case studied previously [2] is used as the testbed for exploring the prediction characteristics of the different SLW gas property models here. That case is the work of Andersson *et al.* [15] reporting oxy-combustion experiments using propane as the fuel. Oxy-combustion is a scenario where accurately treating the contribution of radiative heat transfer is particularly important due to very high concentrations of radiatively participating CO₂. Flue gas was cooled, dried, and re-injected into the furnace as the diluent for the oxygen in place of the nitrogen that was present in air-fired flames. The furnace studied was cylindrical, with a diameter of 0.8 m and length of 2.4 m, and fired downward. Three sets of experimental data were reported by Andersson *et al.*, but two of the experimental conditions reportedly yielded very luminous flames and therefore, radiative transfer in these cases was strongly influenced

by the presence of soot. The remaining case was only slightly luminous, and thus was influenced by soot to a much lesser extent. It is for this latter case that predictions have been made here. The contribution to radiative transfer from soot is assumed to be weak for this case, and is neglected in this study.

The propane burner used in the experiments as described in [15] and summarized in [2] featured a fuel lance (diameter = 34 mm) and two cylindrical feed-gas registers. The primary register was swirled with a fin angle of 45 deg and featured an outer diameter of 52 mm. The secondary register was swirled with a fin angle of 15 deg and had an outer diameter of 92 mm. For the case simulated here the recycled flue gas was 21% oxygen (by volume) when it was injected into the burner at 300 K. The flow rate for the primary oxidant register was 37 m³/h at standard conditions and for the second register was 54 m³/h at standard conditions. Enough fuel was injected to reach a stoichiometric ratio of 1.15. The walls of the furnace were refractory-lined, and four cooling tubes of unknown dimensions and temperatures were inserted axially along the walls and equally spaced circumferentially in the furnace, to cool the flame. Wall temperature and emissivity were not reported in the study. Consequently, the effective wall temperature from these two effects was assumed arbitrarily to be 873 K with gray emissivity of 0.8.

The commercial CFD code Fluent was used to solve numerically the governing equations. Fluent uses the control volume method [16] on unstructured grids to solve numerically the governing conservation equations. An axisymmetric Fluent simulation model was constructed using the conditions described above for the sake of simplicity. The swirl was included by imposing axial and tangential components of the inlets near the fin angles given in the paper. The mass flow inlets for both fuel and oxidizer were set to 300 K with mass flow rates as described above. The flow field was assumed to be turbulent and the standard $k - \varepsilon$ model was used to model the turbulence. The chemical reaction was modelled using a simple two-step propane combustion model:



The eddy dissipation model was used for turbulence-chemistry interaction.

When performing radiation heat transfer calculations, Fluent provides several RTE solution methods, and the finite volume variant of the Discrete Ordinates (DO) model was used here. The DO radiation model was employed with 4 divisions in the θ and ϕ directions, 2 pixels in θ and ϕ .

The default model for determining the radiative properties of gases in Fluent is the Domain Based WSGG model. Fluent has built-in coefficients for the 4-RTE WSGG formulations. They are taken from Smith *et al.* [17] and Coppalle and Vervisch [18]. The coefficients from Smith *et al.* were calculated for $p_{CO_2} = 0$ (partial pressure of CO₂), $p_{H_2O} = 0$ (partial pressure of water vapor), $p_{H_2O} = 1$ atm, $p_{H_2O}/p_{CO_2} = 1$, and $p_{H_2O}/p_{CO_2} = 2$. These data are valid for $p = p_{H_2O} + p_{CO_2} = 1$ atm (total pressure), and temperatures between 600 K and 2400 K. The coefficients of Coppalle and Vervisch used by Fluent have been developed for $p_{H_2O}/p_{CO_2} = 1$ and $p_{H_2O}/p_{CO_2} = 2$ with valid temperature range between 2500 K and 3000 K. Based on the temperature and species partial pressures in the mixture Fluent chooses the closest data. Between 2400 K and 2500 K, Fluent interpolates the two sets of data linearly with temperature. For p other than 1 atm Fluent uses scaling rules from Edwards and Matavosian [19], which presents scaling data for total pressure of 0.1 atm, 0.3 atm, 3 atm and 10 atm at temperature of 800 K, 1200 K, 1600 K, and 2000 K.

Instead of solving four RTEs as formulated by the original WSGG formulation, Fluent's Domain Based WSGG model solves only one RTE to reduce the computational effort. Fluent uses the WSGG coefficients to calculate the gas mixture total emissivity ε . Once the gas emissivity is obtained, a single gray gas mixture absorption coefficient to be used in the RTE

solution is calculated using $\kappa = -(1/L_e) \ln(1 - \varepsilon)$ where $L_e = 3.6V_{tot}/A_{tot}$ and V_{tot} is the total volume and A_{tot} is the total surface area of the simulation domain.

Fluent allows users to solve multiple RTEs via a User Defined Function (UDF) and provide macros for the implementation. The SLW model by itself is very flexible and can be arranged readily to solve an arbitrary number of RTEs using Fluent's framework. The three variants of the SLW model (RA-SLW, LC-SLW, and RC-SLW models) as described in foregoing sections have been implemented using User Defined Functions. Tabulated ALBDF data were used in all simulations. The multiplication method was applied in the SLW methods to treat the gas mixture [20]. After appropriate grid refinement, the predictions reported here employed 67,611 high quality quad mesh cells with clustering in the flame region. To provide comparison, simulations were performed on the same grid with the RA-SLW, LC-SLW, and RC-SLW gas radiation models, as well as the Fluent Domain Based WSGG model. Further, the influence of the number of gray gases used in the SLW model was explored by performing simulations with $n = 10, 5$, and 3 gray gases for each of the RA-SLW, LC-SLW, and RC-SLW models.

This work will focus on the predicted temperature and radiative heating distributions for the gas spectral property models explored. The radiative heating Q is defined as the radiative source in the energy equation, $Q = -\text{div}(\vec{q}_{rad})$, where \vec{q}_{rad} is the local radiative flux vector.

Results and Discussion

Figure 1 illustrates the predicted temperature (left) and radiative heating (right) for the four gas spectral property models considered here. Only the flame region (1.75 m of furnace length nearest the burner) is shown in the figure. The upper half of each of the six panels illustrates the predictions for the WSGG, LC-SLW, or RC-SLW model, and the lower half shows for comparison the corresponding prediction for the RA-SLW model. All SLW model predictions here used 10 gray gases. Figure 1 reveals that all predictions are qualitatively similar, featuring ignition, a cool curtain due to the introduction of primary and secondary oxidant in the cylindrical registers, a reacting core, and highest temperatures in a cylindrical re-

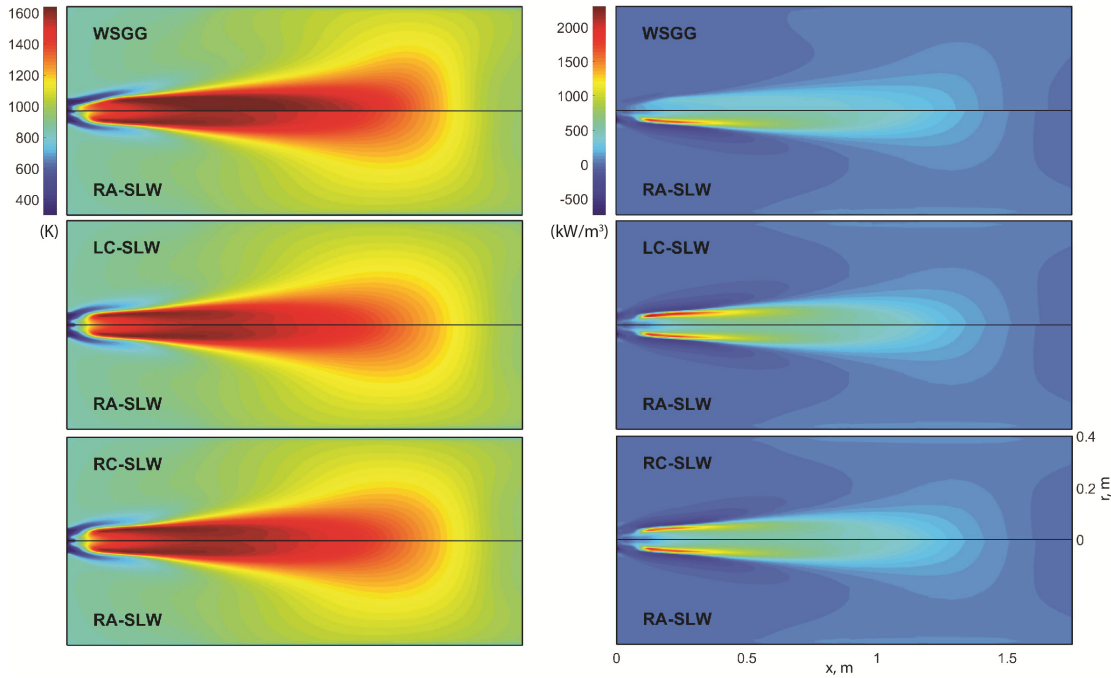


Figure 1: Contours of temperature, K (left) and radiative heating, kW/m^3 (right) for the WSGG and three SLW models. Only the flame zone (1.75 m length) is shown.

gion near the edge of the reaction zone. Only modest differences in predicted temperatures are observed among the three SLW model variants. However as seen in the upper panel (left) the WSGG model yields a significantly different shape of flame zone, with a somewhat flared and blunt flame tip compared to SLW model predictions. Further, there is a substantially larger region of high gas temperature in the flame zone for the WSGG model. It is also seen that the WSGG model predicts earlier ignition and a more conical flame region near the burner than the SLW models. The local radiative heating contours of Fig. 1 (right) show again that the predictions for the three SLW model variants are qualitatively similar. However, the SLW models exhibit a localized region of significantly higher radiative heating on the edge of the flame than the WSGG model. Thus, while all three SLW models produce similar temperature and radiative heating distributions, the predictions differ significantly from those of the rudimentary WSGG model. These differences in WSGG predictions are observed primarily in *i*) the narrowed shape of the flame near the inlet, *ii*) the size of the high-temperature region in the flame core, and *iii*) the blunted shape of the flame downstream of the high temperature reaction zone.

To highlight differences between the various predictions, Fig. 2 shows disparity maps for the WSGG, LC-SLW, and RC-SLW model relative to the RA-SLW model predictions. The local disparity shown is the local difference between a particular model prediction of temperature or radiative heating and the corresponding prediction for the RA-SLW model. For example, the upper left panel shows contours of predicted temperatures for the WSGG model minus the prediction from the RA-SLW model. This highlights the quantitative differences in predictions among the various gas spectral property models employed.

The temperature disparity contours of Fig. 2 (left) reveal that the WSGG predictions are as much as 600 deg K lower at the edge of the flame zone, and modestly higher (perhaps 200 deg K) near the burner exit than the RA-SLW model. The conical cold zone near the burner observed in the temperature contours of Fig. 1 for the WSGG model is also see clearly in Fig.

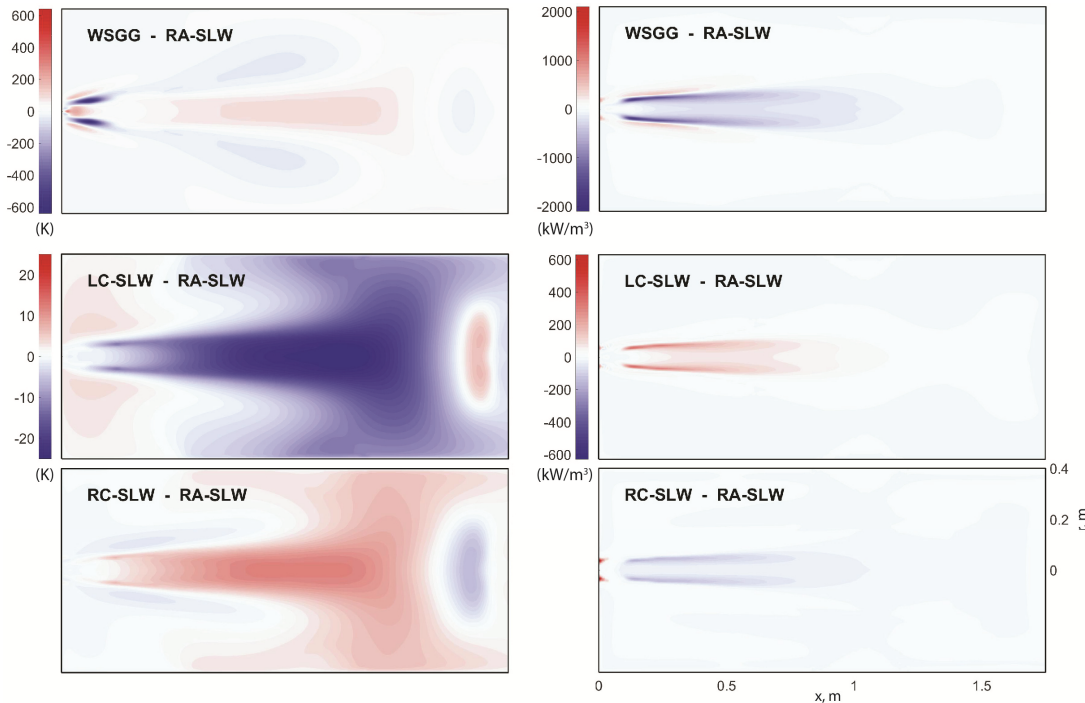


Figure 2. Disparity contours for temperature (left) and radiative heating (right) comparing the WSGG, LC-SLW, and RC-SLW models relative to the RA-SLW method.

2. The LC-SLW model yields predictions of local temperature similar to the RA-SLW model early in the flame, with modestly lower temperatures (15 – 20 deg K) later. (Note the change of scale in the lower two panels of Fig. 2.) Finally, RC-SLW model predictions for temperature are nearly identical to those of the RA-SLW model early, and somewhat higher in the flame core downstream.

The radiative heating disparity maps of Fig. 2 (right) illustrate that the WSGG model predictions are dramatically lower than the RA-SLW model—as much as 1000 kW/m³ at the edge of the flame. The predicted radiative heating for the LC-SLW model is higher at the edge of the flame by perhaps 300 kW/m³. The lower right panel suggests that differences in predictions of radiative heating for the RC-SLW and RA-SLW models is rather modest, near 150 kW/m³ in the cylindrical reaction zone and much lower elsewhere in the furnace.

While the 600 deg K difference in temperature observed in the top panels of Fig. 2 for the WSGG and RA-SLW models is largely due to the difference in predicted flame shape near the inlet. Figure 3 shows radial profiles of temperature and radiative heating in the flame zone, $x = 0.1$ m. These profiles illustrate quite clearly the predicted differences in the shape of the reaction zone and correspondingly higher maximum temperatures, and lower flame-core temperature near the burner predicted by the SLW models relative to the WSGG model. Indeed, one may conclude that to accurately resolve ignition and flame zone shape and corresponding temperature and radiative heating one must adopt more sophisticated property models for the radiation transfer in the gases.

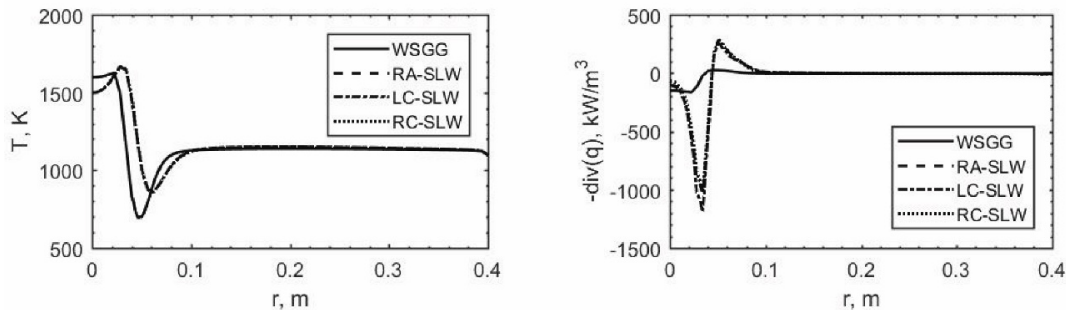


Figure 3. Radial profiles of temperature (left) and radiative heating (right) at $x = 0.1$ m.

Figure 2 also reveals that the LC-SLW model predicts temperatures in the flame region nearly 25 deg K lower than that predicted by the RA-SLW model, while the RC-SLW model predicts temperatures around 15 deg K higher than the RA-SLW model. These observations may be quantified from disparities in temperature and radiative heating displayed in Fig. 2 as the normalized Average Difference and Maximum Difference in predictions, calculated from local temperature T and local radiative heating $Q = -\text{div}(\vec{q}_{rad})$ distributions as follows

$$\text{Avg Diff} = \frac{\int_V |T - T_{ref}| dV / V_{tot}}{\int_V T_{ref} dV / V_{tot}} \quad \text{and} \quad \text{Max Diff} = \frac{\max(|T - T_{ref}|)}{\int_V T_{ref} dV / V_{tot}} \quad (13)$$

$$\text{Avg Diff} = \frac{\int_V |Q - Q_{ref}| dV / V_{tot}}{\max(|Q_{ref}|)} \quad \text{and} \quad \text{Max Diff} = \frac{\max(|Q - Q_{ref}|)}{\max(|Q_{ref}|)} \quad (14)$$

Here, the subscript “*ref*” refers to the reference simulation against which the normalized Average Difference and Maximum Difference are compared in the calculation. It may be mentioned that while other normalizations may be proposed, these metrics are sufficient to illustrate the aggregate differences in predictions among the various models.

Table 1 shows the normalized Average and Maximum Difference for the WSGG, LC-SLW, and RC-SLW model predictions relative to the RA-SLW model. The table reveals, as expected, that the WSGG model yields large Average and Maximum Differences relative to the RA-SLW model. By contrast, the Maximum and Average Differences between LC-SLW and RC-SLW models and the corresponding RA-SLW model predictions are much smaller. Note that while Figs. 1-3 reveal that the WSGG model prediction differs significantly from the SLW models in the flame region, Table 1 suggests that the Average Differences in temperature and radiative heating relative to the RA-SLW predictions are quite modest, 1.8% and 0.36%, respectively. While these magnitudes are due in large part to the choice of normalization, the cylindrical geometry of the furnace also plays a factor, weighting the values near the wall higher than those near the core of the flame where differences are most prominent.

Table 1. Normalized Average Difference and Maximum Difference in predicted temperature and radiative heating relative to the RA-SLW model.

Method	Temp. Diff.*		Rad. Heat. Diff.*	
	Max	Avg	Max	Avg
WSGG	63.9%	1.8%	92.8%	0.36%
LC-SLW	2.5%	0.5%	19.6%	0.05%
RC-SLW	1.2%	0.2%	35.0%	0.11%

*Relative to RA-SLW model

To investigate the robustness of each of the SLW model formulations, the number of gray gases n used in all methods was varied, with predictions carried out for $n = 10$, 5, and 3. While a higher number of gray gases used in the SLW model simulation yields greater accuracy, there is an attendant increase in computation time, as will be shown later. Thus, it is desirable to understand how the predictions vary with the number of gray gases used, and more practically, how few gray gases may be employed and still achieve accurate results. The results of these simulations are illustrated in Fig. 4, where the number of gray gases used in each model is denoted by the subscript for each of the SLW models. The upper half of each panel illustrates contours of temperature or radiative heating for a simulation using n gray gases (3 or 5), and the lower half of each panel shows the corresponding prediction using $n = 10$ gray gases in the same SLW model. Thus, one can compare the difference in predictions as n is reduced.

The temperature contour data of Fig. 4 (left panels) reveal only modest differences in temperature between the $n = 5$ predictions and the $n = 10$ predictions for the RA-SLW, LC-SLW, and RC-SLW models. Reducing the number of gray gases to $n = 3$, however, yields considerable differences. In the 3-gray-gas results the RA-SLW and LC-SLW models predict more flared and blunt flame zones, with a larger region of localized higher gas temperatures at the edge of the flame. Indeed, one may see that the flame zone is both longer and wider for the RA-SLW and LC-SLW models as the number of gray gases is reduced. By contrast, the Rank Correlated SLW model temperature prediction exhibits only modest dependence on the number of gray gases. The radiative heating contours in Fig. 4 (right panels) show trends in model prediction dependence on n . The localized region of high radiative heating at the edge of the flame zone reveals higher values of Q as the number of gray gases is reduced for the RA-SLW and LC-SLW models. The RC-SLW model, however, exhibits very little difference in the radiative heating contours as n is reduced from 10 to 5 and 3.

The differences observed in Fig. 4 are further highlighted in Fig. 5 by disparity contours comparing predicted profiles using $n = 3, 5$, and 10 gray gases. The disparity maps show the difference in prediction of local temperature and local radiative heating between simulations employing a different number of gray gases. Figure 5 reveals that in the case of the RA-SLW and LC-SLW approaches the largest effect on the predicted thermal structure of the flame is observed downstream, while the largest effect on flux divergence is observed near the inlet

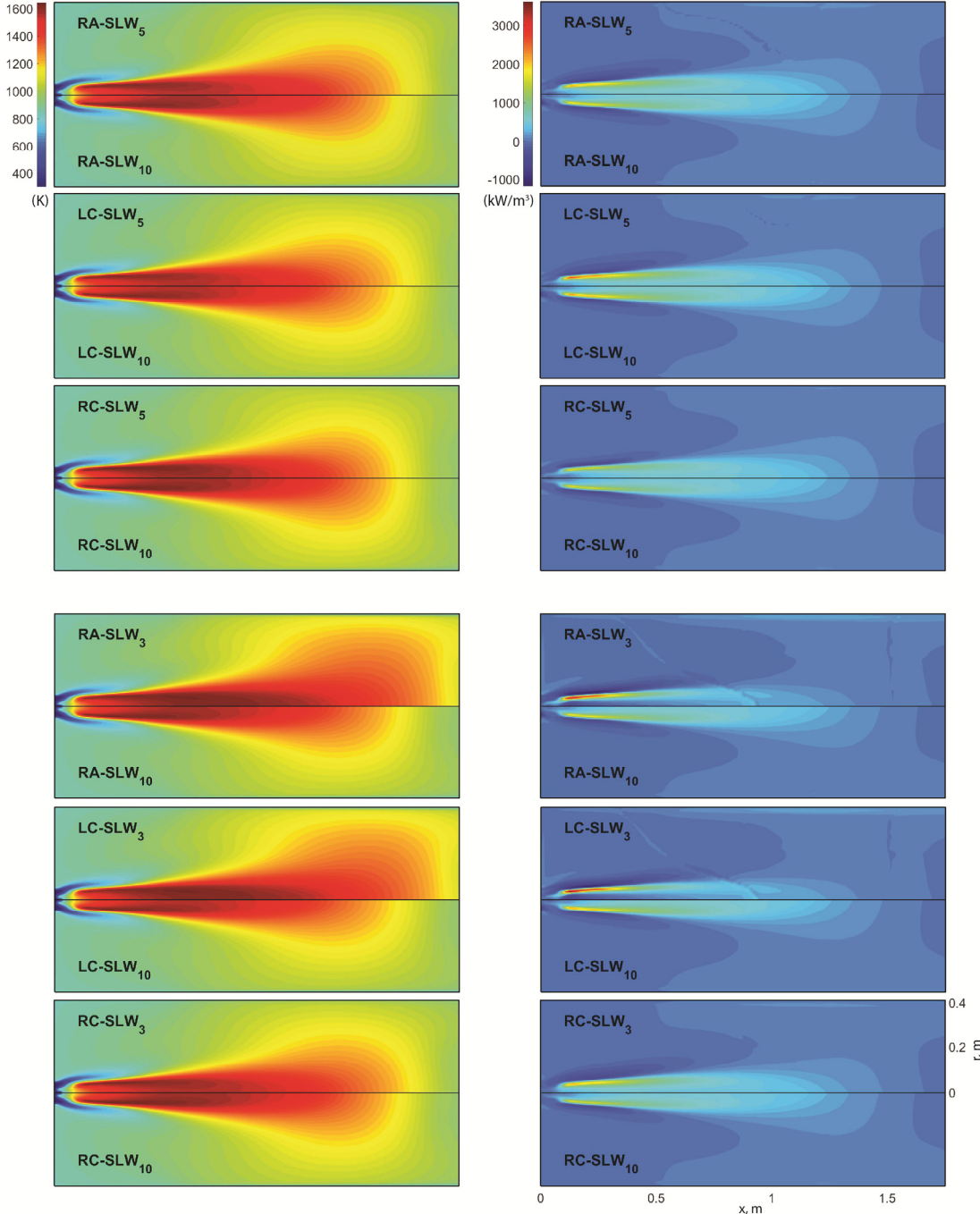


Figure 4. Contours of predicted temperature (left) and radiative heating (right) for $n = 3$, 5 , and 10 gray gases. The lower half of each panel shows the 10 -gray-gas case.

where large thermal gradients are present. In the case of the RC-SLW approach, however, only modest differences in the predicted temperature fields are observed for $n = 10, 5$, and 3 gray gases, with differences observed only near the furnace wall when 3 gray gases are used. Similar observations may be made relative to the local radiative heating. The magnitude of the predicted local radiative heating changes quite significantly for the RA-SLW and LC-SLW models as n is reduced from 10 to 5 , with differences in Q as high as 700 kW/m^3 (both

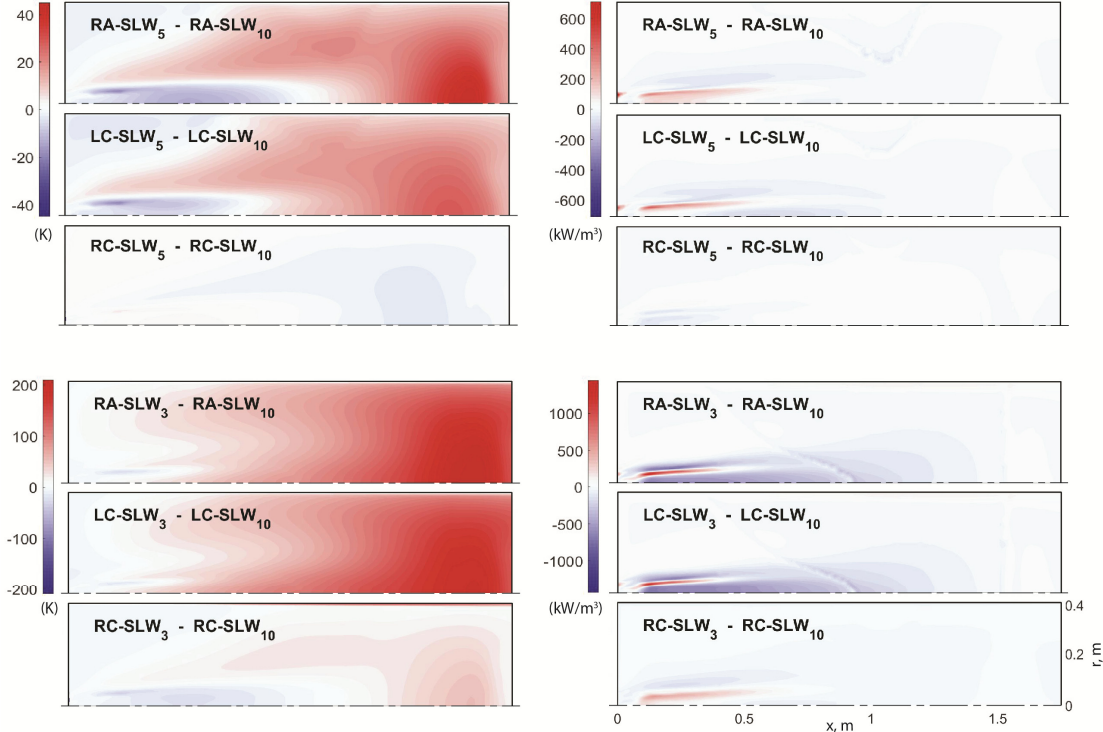


Figure 5. Disparity contours for temperature (left) and radiative heating (right) comparing the 3- and 5-gray-gas predictions to the corresponding 10-gray-gas predictions.

higher and lower) observed. By contrast, the predicted radiative heating for the RC-SLW model is largely independent of the number of gray gases for $3 < n < 10$.

It is worth mentioning that while each of the 5-gray-gas SLW model predictions produced quantitatively similar results to their corresponding 10-gray-gas counterparts, both the RA-SLW and LC-SLW models required that the energy and discrete-ordinates under-relaxation factors be significantly reduced to reach a converged solution. The 3-gray-gas RA-SLW and LC-SLW predictions both required a further reduction of under-relaxation factors to reach a converged solution. For the 3-gray-gas simulations with the RA-SLW and LC-SLW models the predicted fields ceased changing with iterations in the numerical solution, but the residuals oscillated somewhat about levels higher than that found in either the $n = 5$ or 10 solutions. By contrast, the RC-SLW model was well-behaved numerically when both 3 and 5 gray gases were used and, notably, without requiring adjustment of the under-relaxation factors.

Finally, Table 2 compares the average computation time per iteration for all models (HP Elitedesk 800 G4 with Intel i5-8500 processor at 3.0 GHz, 6 cores), as well as the normalized Average and Maximum Difference in T and Q relative to the 10-gray-gas simulation for the three SLW model variants studied. The table illustrates that the Average and Maximum Differences in both temperature and radiative heating increase with a reduction of the number of

gray gases. The increases are quite significant for the RA-SLW and LC-SLW models, whereas the Differences for the RC-SLW model reflect a more modest dependence on n .

Table 2. Computational expense and normalized Average and Maximum Difference data relative to the $n = 10$ simulation for each of the gas spectral property models.

Model	n	Time/Iter. (s)	Temp. Diff.*		Rad. Heat. Diff.*	
			Max	Avg	Max	Avg
WSGG	1	0.2	—	—	—	—
	10	2.0	—	—	—	—
RA-SLW	5	1.2	4.1%	1.0%	36.7%	0.16%
	3	0.7	20.8%	7.5%	74.7%	0.58%
LC-SLW	10	2.1	—	—	—	—
	5	1.1	2.9%	0.9%	20.3%	0.12%
RC-SLW	3	0.6	19.2%	7.7%	58.1%	0.48%
	10	2.9	—	—	—	—
RC-SLW	5	1.6	0.8%	0.2%	4.0%	0.04%
	3	1.0	16.2%	1.2%	31.4%	0.24%

*Relative to 10-gray-gas predictions

The computation time shown in Table 2 reveals that when n gray gases are used, the computational expense of the RA-SLW and LC-SLW models is approximately n times greater than that of the WSGG model, while the RC-SLW model is nominally $1.5n$ greater than the computational expense of the WSGG model.

The data of Figures 4 and 5 and Table 1, and the observations regarding numerical stability of the SLW models noted previously suggest that the RC-SLW model is more robust than either of the other two SLW model variants. Stated more succinctly, while the RC-SLW model requires slightly more computational expense than the RA-SLW and LC-SLW models, it shows robust and accurate behavior even when only a small number of RTEs are used. The increased stability and accuracy of this method show a clear advantage over the RA-SLW and LC-SLW methods in comprehensive combustion simulations.

Conclusions

The Reference Approach SLW, Locally Correlated SLW, and Rank Correlated SLW gas spectral property models have been implemented in Fluent, a comprehensive modeling strategy for prediction of turbulent reacting flow. Predictions for these three models are compared to those using the Domain Based Weighted-Sum-of-Gray-Gases Model. The three SLW model variants yield predictions that are quite similar qualitatively and quantitatively, but which differ significantly from predictions using the WSGG model. Each of the SLW model formulations appears to have strengths. The RA-SLW and LC-SLW model predictions show significantly greater dependence on the number of gray gases employed. The RC-SLW Model is the most robust.

References

- [1] Denison, M.K., Webb, B.W. "A spectral line-based weighted-sum-of-gray-bases model for arbitrary RTE solvers," *ASME J. Heat Transfer*, 115: 1004-1012 (1993)

- [2] Webb, B.W. Ma, J., Pearson, J.T., Solovjov, V.P., "SLW modeling of radiation transfer in comprehensive combustion predictions," *Comb. Sci. Tech.*, 190:1392-1408 (2018).
- [3] Nguen, P.D., Danda, A., Embouazza, M., Gazdallah, M., Evrards, P., Feldheim, V., "Application of the spectral line-based weighted-sum-of-gray-gases model (SLWSGG) to the calculation of radiative heat transfer in steel reheating furnaces firing on low heating value gases," *J. Phys.: Conf. Ser.*, 369:012008 (2012).
- [4] Garten, B., "Detailed radiation modeling of a particle-oxidation flame," *Int. J. Therm. Sci.*, 87:68-84 (2015).
- [5] Rebola, A., Azevedo, J.L.T., "Modelling pulverized coal combustion using air and O₂+recirculated flue gas as oxidant," *Appl. Thermal Eng.* 83:1-7 (2015).
- [6] Krishnamoorthy, G., Sami, M., Orsino, S., Perera, A., Shahnam, M., Huckaby, E.D., "Radiation modeling in oxy-fuel combustion scenarios," *Int. J. Comp. Fluid Dyn.* 24:69-82 (2010).
- [7] Darbandi, M., Barezban, M.B., Schneider, G.E., "Evaluating the ability of SLW model in numerical simulation of radiative turbulent reacting flow in industrial application," *Proc. 5th Joint US-European Fluids Eng. Conf.*, July 15-20, Montreal, Quebec, 2018.
- [8] Solovjov, V.P., Webb, B.W., André, F. "Radiative Properties of Gases," *Handbook of Thermal Science and Engineering*, ed. F. Kulacki, Springer, New York, vol. 2, pp. 1-74, 2018.
- [9] Denison, M.K., Webb, B.W., "The spectral line based weighted-sum-of-gray-gases model in non-isothermal non homogeneous media," *ASME J. Heat Transfer*, 117:359-365 (1995).
- [10] Solovjov, V.P., André, F., Lemonnier, D., Webb, B.W. "The generalized SLW model," *Eurotherm105: Computational Thermal Radiation in Participating Media V*, *J. Phys.: Conf. Ser.*, 012022, 676:1-36 (2016).
- [11] Pearson, J.T., Webb, B.W., Solovjov, V.P., Ma, J., "Efficient representation of the absorption line blackbody distribution function for H₂O, CO₂, and CO at variable temperature, mole fraction, and total pressure," *J. Quant. Spectr. Rad. Transfer*, 138:82-96 (2014)
- [12] Solovjov, V.P., André, F., Lemonnier, D., Webb, B.W., "The rank correlated SLW model of gas radiation in non-uniform media," *J. Quant. Spectr. Rad. Transfer*, 197:26-44 (2017).
- [13] André, F., Solovjov, V.P., Lemonnier, D., Webb, B.W., "Co-monotonic global spectral models of gas radiation in nonuniform media based on arbitrary probability measures," *J. Appl. Math. Modeling*, 50: 741-754 (2017).
- [14] Solovjov, V.P., Webb, B.W., André, F., Lemonnier, D., "The locally correlated SLW model of gas radiation in non-uniform media," *Proc. 9th Int'l. Symp. Rad. Transfer*, Athens, Greece, June 3-7, 2019, Begell House.
- [15] Andersson, K., Johansson, R., Johnsson, F., Leckner, B., "Radiation intensity of propane-fired oxy-fuel flames: Implications for soot formation," *Energy Fuels*, 22:1535-1541 (2008).
- [16] Patankar, S.V., *Numerical Heat Transfer and Fluid Flow*, Hemisphere, 1980.
- [17] Smith, T.F., Shen, Z.F., Friedman, J.N., "Evaluation of coefficients for the weighted sum of gray gases model," *ASME J. Heat Transfer*, 104:602-608 (1982).
- [18] Coppalle, A., Vervisch, P., "The total emissivity of high-temperature flames," *Combust. Flame*, 49:101-108 (1983).
- [19] Edwards, D.K., Matavosian, R., "Scaling rules for total absorptivity and emissivity of gases," *ASME J. Heat Transfer*, 106:684-689 (1984).
- [20] Denison, M.K., Webb, B.W., "The spectral-line weighted-sum-of-gray-gases model for H₂O/CO₂ mixtures," *ASME J. Heat Transfer*, 117:788-798 (1995).